RSM-OPTIMIZED MARINE BACTERIAL MELANIN-CONJUGATED LIPID MAGNETIC NANOPARTICLES AND ITS IN VITRO APOPTOSIS INDUCTION, CONTROLLED RELEASE, AND IN VIVO PHARMACOKINETIC EVALUATION

Shilpa Valiyaparambil[1]*, Janakiraman Kunchithapatham[1], Vinod K.R[2], Venkatesan P[1], Suresh B[3]. Muddukrishnaiah Kotakonda[4]

[1]Department of Pharmacy, Annamalai University, Annamalai Nagar, Chidambaram-608002, Tamil Nadu, India.
[2]Department of Pharmaceutics, Sanjo College of Pharmaceutics Studies, Vellapara, Palakkad, Kerala, India.
[3]Department of Chemical Engineering, Annamalai University, Annamalai Nagar, Chidambaram-608002, Tamil Nadu, India.
[4]Department of Pharmaceutics, Jamia Salafiya Pharmacy College, Pulikkal, Malappuram, Kerala, India

Correspondence Author:
Mrs. Shilpa Valiyaparambil,
Department of Pharmacy,
Annamalai University, Annamalai Nagar, Chidambaram-608002,
Tamil Nadu, India.
Email: shilpavp24@gmail.com

Abstract

Introduction: Marine bacterial pigment polymers are remarkable bioactive compounds with significant potential for disease treatment. RSM-Optimized marine bacterial Melanin-Conjugated Lipid Magnetic Nanoparticles and its In Vitro Apoptosis Induction, Controlled Release, and In Vivo Pharmacokinetic Evaluation. **Methodology:** Melanin was isolated from *Actinoalloteichus cyanogriseus* and conjugated to lipid magnetic nanoparticles. Optimisation done by using a response surface methodology (RSM) with central composite design (CCD). M-C-L-M-NPs characterized particle size and zeta potential, UV-Vis, FTIR, FE-SEM, HR-TEM, BET, and ICP-OES. *In vitro* anticancer efficacy was assessed by AO/EB staining and quantitative RT-PCR for apoptosis-related gene expression. *In-vitro* release of melanin from M-C-L-M-NPs suspension was evaluated in phosphate buffer (pH 7.4) for 24 h (n=3). Data were fitted to zero-order, first-order, Higuchi, and Korsmeyer–Peppas models. Sterility followed IP/USP incubation. Acute toxicity, organ histology, pharmacokinetic evaluation were assessed. **Results**: RSM identified 11.366 mg melanin and 5.000 mg lecithin as the model-predicted optimum, with predicted particle size of 80.052 nm, zeta potential of 32.0 mV, and desirability of 0.910. Experimental characterization showed a hydrodynamic diameter of 89.2 nm, polydispersity index of 0.31, and zeta potential of −30.2 mV, HR-TEM showed a size range of 24–63 nm. BET surface area analysis of M-C-L-M-NPs revealed a specific surface area of 96.9 m^2/g, with mesoporous structure confirmed by Type IV isotherms and BJH analysis, indicating both nano and mesopores ideal for drug delivery. ICP-OES quantification showed reliable iron loading, inside the nanoparticles**.** Inhibition assays demonstrated a potent, dose-dependent SK-MEL-3 cell cytotoxicity (IC_{50}: 19.1 ± 1.5 µg/mL). Treated cells showed increased apoptosis, with gene expression analysis revealing upregulation of BAX (1.91-fold) and BAD (2.77-fold), and downregulation of BCL2 (0.87) and AKT. Release remained controlled with 9.97% at 1 h and 75.20% at 24 h. Higuchi ($r^2 = 0.987$) and Korsmeyer–Peppas ($r^2 = 0.993$; n = 0.673) dominated. M-C-L-M-NPs-Suspension was sterile and non-toxic with normal liver/kidney morphology. Cmax increased to 29.6 µg/mL, persisting 10.4 µg/mL at 24 h. M-C-L-M-NPs possess finely tunable physical properties and robust pro-apoptotic anticancer activity *in-vitro*. **Discussion**: M-C-L-M-NPs exhibited favorable nanoscale characteristics (88.5 nm; 30.8 mV), high surface area (96.9 m^2/g), and mesoporosity supporting drug delivery. Reliable iron incorporation, sustained release (75.20% at 24 h), significant SK-MEL-3 cytotoxicity (IC_{50} 19.1 µg/mL), apoptosis induction, biocompatibility, and enhanced pharmacokinetics collectively demonstrate promising anticancer potential. **Conclusion:** M-C-L-M-NPs-Suspension provided reproducible diffusion-controlled release with 75% liberation at 24 h. Safety was verified by sterility, absence of acute toxicity, and normal histology supporting their potential as

innovative nanocarriers for melanoma therapy.

Keywords: Marine bacterial melanin; melanin–lecithin magnetic nanoparticles; melanoma; SK-MEL-3; response surface methodology; apoptosis; drug release; pharmacokinetics.

How to cite this article: Valiyaparambil, S., Kunchithapatham, J., K. R., V., P., V., B., S., & Kotakonda, M. (2026). RSM-optimized marine bacterial melanin-conjugated lipid magnetic nanoparticles and its in vitro apoptosis induction, controlled release, and in vivo pharmacokinetic evaluation. International Journal of Drug Delivery Technology, 2026;16(87s): 1029-1052; DOI: 10.25258/ijddt.16.87s.107

Introduction

Skin cancer is among the most common forms of cancer, arising from the uncontrolled growth of abnormal skin cells, typically caused by cumulative exposure to ultraviolet (UV) radiation from the sun [1]. The primary types of basal cell carcinoma, squamous cell carcinoma, and melanoma vary in aggressiveness, with melanoma being the deadliest [2]. Early stages of skin cancer commonly present as new, changing skin lesions, and timely detection increases the likelihood of successful treatment [3]. Untreated aggressive skin cancer can lead to serious complications, including local tissue destruction, scarring, and disfigurement. Advanced cases may involve metastasis, where cancer cells spread to lymph nodes and distant organs such as the lungs, liver, and brain, significantly reducing survival chances [4]. Complications also extend to chronic wounds, secondary infections, and psychological distress due to changes in appearance [5]. Therapies like surgery, radiation, and chemotherapy can result in additional side effects, impacting overall quality of life. Marine bacterial pigment polymers are remarkable bioactive compounds with significant potential for disease treatment [6]. Produced by diverse marine bacteria, these natural pigments, such as prodigiosin, violacein, melanin, and carotenoids, exhibit strong antibacterial, anticancer, antiviral, and antioxidant properties [7]. Marine pigment polymers are often biodegradable, non-toxic, and environmentally friendly, making them highly attractive for pharmaceutical development [8]. Their therapeutic activities are wide-ranging: pigments like prodigiosin and violacein can induce apoptosis and inhibit the proliferation of various cancer cell lines. Marine bacterial pigment polymers' unique chemical diversity and bioactivity support their use in developing innovative therapies for various infectious and non-infectious diseases. Due to poor solubility of marine bacterial pigments and restricted permeability across biological membranes, low bioavailability often limits their clinical application. These challenges hinder their effective absorption and reduce their overall therapeutic potential. Marine bacterial pigment polymers hold significant promise as safe and sustainable drug candidates, further research is necessary to enhance their solubility and membrane permeability, ensuring their successful translation from laboratory studies to effective clinical therapies. The present study focuses on the optimized synthesis of marine bacterial melanin-conjugated magnetic nanoparticles and evaluates their in vitro activity against skin cancer.

Materials And Methods

Isolation Of Marine Bacterial Melanin

Marine bacterial melanin was isolated from *Actinoalloteichus cyanogriseus* strain AU-RM-4 according to the previously reported method of Muddukrishnaiah Kotakonda et al. [9]. The strain was cultivated on anaerobic actinomycetes agar for melanin production, resulting in the formation of extracellular black melanin pigment. The pigment was recovered from the culture medium by acid treatment, followed by purification and drying. The obtained melanin was characterized by UV–Vis spectroscopy, and its characteristic absorption profile was compared with that of a commercially available melanin standard [9].

Experimental Design and Formulation Optimization

Central Composite Design

A response surface methodology (RSM)-based central composite design (CCD) was employed for systematic formulation optimization using Design-Expert® version 13 (Stat-Ease Inc., USA). Based on preliminary formulation investigations, melanin concentration (A) and lecithin concentration (B) were selected as the independent formulation variables.

Melanin was investigated over the concentration range of 10–20 mg, while lecithin was evaluated over the range of 5–10 mg. The center-point levels were fixed at 15 mg melanin and 7.5 mg lecithin. An axial distance of $\alpha = 1.41421$ was applied, resulting in axial levels of 7.92893 and 22.0711 mg

for melanin and 3.96447 and 11.0355 mg for lecithin, respectively. The CCD comprised 10 experimental runs, including four factorial points, four axial points, and two center points.

Particle size (Y_1, nm) and zeta potential (Y_2, mV) were selected as the dependent responses because of their relevance to the physicochemical characteristics of the developed formulation. The experimental formulations were prepared according to the randomized design matrix generated by Design-Expert®, while other formulation and processing variables were maintained constant. The prepared formulations were subsequently characterized for particle size and zeta potential. The experimentally obtained response values were entered into Design-Expert® for regression analysis and analysis of variance (ANOVA). Three-dimensional response-surface and two-dimensional contour plots were generated to visualize the individual and interactive effects of melanin and lecithin concentrations. Numerical optimization was subsequently performed using the desirability-function approach to identify the formulation composition providing the desired combination of responses.

Statistical Analysis and Model Development

Quadratic polynomial models were fitted separately to particle size and zeta potential responses. The significance of the individual linear, interaction, and quadratic terms was assessed using ANOVA. Model adequacy was evaluated using the coefficient of determination (R^2), adjusted R^2, predicted R^2, coefficient of variation (CV), standard deviation, and adequate precision. The significance of the regression model was assessed at a 95% confidence level, with $p < 0.05$ considered statistically significant. The quadratic equations generated by Design-Expert® were expressed in terms of both coded and actual factors. Response-surface and contour plots were used to visualize the effects of the formulation variables and their interaction within the investigated design space. Numerical optimization was performed by applying predefined goals and constraints to the independent variables and responses.

Melanin-conjugated lipid Magnetic Nanoparticles (M-C-L-M-NPs) were synthesized using the chemical co-precipitation method.

Melanin-conjugated lipid magnetic nanoparticles (M-C-L-M-NPs) were prepared using a modified chemical co-precipitation and lipid-assembly method adapted from a previously reported procedure by Kumar et al. Briefly, ferric chloride hexahydrate ($FeCl_3 \cdot 6H_2O$) and ferrous sulphate heptahydrate ($FeSO_4 \cdot 7H_2O$) were dissolved separately in distilled water and subsequently combined under a nitrogen atmosphere with continuous stirring at 60–70°C. For the synthesis of magnetite (Fe_3O_4) nanoparticles, the Fe^{3+2+} molar ratio was maintained at 2:1. Accordingly, the quantities of the iron salts were adjusted to achieve the required stoichiometric ratio. Aqueous ammonia was added gradually under vigorous stirring until the reaction pH reached approximately 10, facilitating the co-precipitation of iron oxide nanoparticles. Citric acid was subsequently added as a surface-stabilizing agent, and the suspension was stirred for an additional 30 min. The resulting citrate-stabilized magnetic nanoparticles were collected by magnetic separation and washed repeatedly with distilled water to remove residual soluble components. The nanoparticles were subsequently dried at 60°C or lyophilized, depending on the intended application.

For the preparation of the melanin–lecithin lipid nanostructure, melanin and lecithin were used in the proportions specified by the experimental formulations generated using Design-Expert® version 13 (Stat-Ease Inc., USA). The lipid phase was gradually introduced into the aqueous surfactant phase under high-speed homogenization at 10,000–15,000 rpm, according to the formulation conditions listed in Table 1. The organic solvent was subsequently removed under reduced pressure with continuous stirring to obtain the melanin–lecithin nanoparticle suspension. The previously prepared

citrate-stabilized magnetic nanoparticles were then incorporated into the suspension under controlled stirring to facilitate their association with the melanin–lecithin nanostructure. The resulting M-C-L-M-NPs suspension was subjected to magnetic separation and repeated washing to remove unbound or loosely associated components. The final formulation was stored at 4°C until further characterization

Table 1: Composition of different formulations (F1, F2, and F3) containing ferric chloride hexahydrate, ferrous sulphate heptahydrate, melanin, and lecithin, with pH adjustment and distilled water as required.

Ingredient	F1	F2	F3
$FeCl_3 \cdot 6H_2O$	5 g	5 g	5 g
$FeSO_4 \cdot 7H_2O$	5 g	5 g	5 g
Melanin	10 mg	15 mg	20 mg
Lecithin	5 mg	7.5 mg	10 mg
Citric acid	10	10	10
NH_4OH	150	150	150
NaOH	q.s. to pH 10	q.s. to pH 10	q.s. to pH 10
Distilled water	Qs	Qs	Qs

Characterization of M-C-L-M-NPs

M-C-L-M-NPs were characterised using UV-Vis spectroscopy for surface plasmon resonance analysis, with a BioSpec Nano (Shimadzu). Functional group confirmation was identified using ATR-FTIR spectroscopy. FE-SEM (TESCAN) and HR-TEM (JEOL) examined surface features and microscopic properties. Particle size distribution and zeta potential of M-C-L-M-NPs were measured using Malvern Zetasizer Nano ZS. Surface area was measured by nitrogen adsorption at 77.35 K after degassing a 0.3361 g sample at 200°C for 2.3 hours, using a Quantachrome Autosorb iQ and BELSORP MAX analyzer; the BET method determined surface area, while NLDFT for cylindrical pores provided pore size distribution from the isotherm data. A 200 mg M-C-L-M-NPs sample is mixed with 8 ml concentrated HNO3 and digested in a microwave digester at 190°C for 45 minutes. After digestion, 200 µl is diluted to 10 ml with 2% HNO3, filtered, and analyzed using ICP-OES (Avio 200-Parkin Elmer instrument) [12].

***In Vitro* Anticancer Activity of M-C-L-M-NPs Against SK-MEL-3 Cells.**

SK-MEL-3 skin cancer cells were seeded at 1×10^4 cells per/mL in 96-well plates and allowed to adhere for 24 hours. Cells were then treated with varying concentrations (5 - 40 µg/ml) of M-C-L-M-NPs and incubated for another 24 hours at 37°C with 5% CO_2. After treatment, MTT dye (5 mg/ml in PBS) was added and incubated for 4 hours [13]. The formazan crystals formed were dissolved in 100 µl DMSO, and absorbance was measured at 540 nm. Cell viability was determined relative to control cells, and IC_{50} values were calculated from dose-response curves (n=3).

Measure M-C-L-M-NPs apoptotic induction in SK-MEL-3 Cells.

SK-MEL-3 cells treated with M-C-L-M-NPs were assessed for apoptosis using acridine orange/ethidium bromide dual staining. Acridine orange stains all cells green by binding to DNA, while ethidium bromide penetrates only nonviable cells, producing red fluorescence by intercalating with DNA, allowing identification of apoptotic cells.

Quantitative Real-time PCR (Gene expression).

Total RNA was isolated from both M-C-L-M-NPs-treated and untreated SK-MEL-3 cells using the RNeasy kit (Qiagen, USA) following the manufacturer's instructions. The mRNA expression of four target genes (primer sequences in Table S1) was then analyzed by quantitative real-time PCR (qPCR) on the Rotor-Gene Q 5plex HRM

system, using QuantiNova Reverse Transcription and SYBR-Green mix (Qiagen, USA). The thermal protocol included 95°C for 3 minutes, followed by 40 cycles of 95°C for 30 seconds, annealing/extension at 58.1°C, and a final step at 60°C for 20 seconds. Beta-actin served as the reference gene, and relative gene expression was calculated using the comparative Ct method, with all reactions performed in duplicate.

Preparation of M-C-L-M-NPs-Suspension

The M-C-L-M-NPs suspension was prepared by sequential high-shear and high-pressure homogenization. Briefly, Polysorbate 80 (1% w/v) was dissolved in Milli-Q water under magnetic stirring at 500 rpm for 30 min at 25 °C to obtain the stabilizing aqueous phase. The preformed M-C-L-M-NPs were gradually incorporated into the stabilizing medium under continuous stirring to obtain a coarse dispersion. The dispersion was vortex-mixed for 2 min to facilitate wetting and preliminary deagglomeration and was subsequently subjected to high-shear homogenization using homogenizer at 10,000 rpm for 5 min to obtain a uniform predispersion. The resulting predispersion was then processed using a high-pressure homogenizer at 1000 bar for 20 cycles at 25 °C to further reduce particle size and improve dispersion uniformity. The homogenized suspension was visually examined for uniformity and the absence of visible aggregates. The final suspension was aseptically passed through a 0.22 µm PVDF membrane, filled into sterile amber glass vials, sealed, and stored at 4 °C until further use. Sterility of the final M-C-L-M-NPs suspension was evaluated by the membrane-filtration method according to the applicable pharmacopoeial sterility test. The sterile suspension was subsequently subjected to physicochemical characterization and further evaluation

***In-Vitro* drug release study of M-C-L-M-NPs-Suspension**

The in-vitro release profile of M-C-L-M-NPs-Suspension was assessed using the dialysis membrane diffusion technique. A precise amount of the formulation was enclosed in a pre-swollen dialysis bag, which was then submerged in phosphate buffer (pH 7.4) at a controlled temperature of 37 ± 0.5 °C with constant magnetic stirring. Aliquots were collected at fixed time points over 24 hours and replenished with equal volumes of fresh buffer to maintain sink conditions. Melanin concentration in the samples was quantified via UV-visible spectrophotometry, enabling the computation of cumulative percentage drug release as a function of time.

Drug release kinetics of M-C-L-M-NPs-Suspension

To analyse the *in-vitro* release mechanism of M-C-L-M-NPs-Suspension, cumulative percentage drug release (Q_t) data were fitted to four kinetic models using linear regression in Prism software. The zero-order model ($Q_t = k_0 t$) describes constant release rate independent of concentration. The first-order model ($\ln(100 - Q_t) = \ln Q_0 - k_1 t$) indicates concentration-dependent release. The Higuchi model ($Q_t = k_H \sqrt{t}$) evaluates diffusion-controlled matrix systems. The Korsmeyer-Peppas model ($\ln Q_t = \ln k_{KP} + n \ln t$) characterizes release exponent n, where $n < 0.43$ signifies Fickian diffusion, $0.43 < n < 0.85$ suggests anomalous transport, and $n > 0.85$ indicates Case-II relaxation. Model selection was based on highest R^2 (≥0.95) and lowest AIC values, confirming the dominant release mechanism.

Sterility study of M-C-L-M-NPs-Suspension

Sterility assessment of the M-C-L-M-NPs-Suspension followed Indian Pharmacopoeia (IP) and United States Pharmacopoeia (USP) standards via membrane filtration. The sterile filtration assembly, including the unit and holder, was pre-sterilized. Using aseptic technique, nanosuspension samples were filtered through a 0.45 µm sterile membrane under mild vacuum, capturing potential microbes on its surface. The filter was rinsed with sterile 0.9% saline to eliminate inhibitory formulation residues. Each membrane was bisected: one half placed in Fluid Thioglycolate Medium (FTM) at 30–35 °C, the other in Soybean Casein Digest Medium (SCDM) at 20–25 °C. Both were monitored daily for 14 days for turbidity or growth; no visible microbial development confirmed formulation sterility per IP/USP criteria.

***In-Vivo* Pharmacokinetic Studies of M-C-L-M-NPs-Suspension**

Acute toxicity M-C-L-M-NPs-Suspension

Acute intravenous toxicity [14] of the M-C-L-M-NPs suspension was assessed in Wistar albino rats in accordance with OECD guideline 423 and asper the approval of CPCSEA. Asper the institutional ethical approval, healthy Wister albino rats were acclimatized for one week under controlled temperature, humidity, and light–dark conditions with free access to food and water. After overnight fasting, Wister albino rats received a single tail-vein administration of freshly prepared M-C-L-M-NPs suspension at escalating doses ranging from 5 to 2000 mg/kg, alongside a saline control. Animals were monitored intensively during the first hrs post-injection and daily for 14 days to record survival. At study completion histological evaluation conducted to identified for organ toxicity.

***In Vivo* Pharmacokinetic Evaluation of the M-C-L-M-NPs Suspension**

Approval from the IAEC (JSPC/IAEC/05/12/14-2025) and in compliance with CPCSEA regulations, pharmacokinetic experiments were conducted in male Wistar rats weighing 200–250 g (n = 6 per group). Rats acclimatized 7 days (25±2°C, 55±5% RH, 12 h light/dark cycle; ad libitum diet/water) before receiving single IV tail-vein injections (2 mL/kg) under isoflurane anesthesia: Group I (saline control), Group II (free melanin; 10 mg/kg), Group III (MC-MNPs nanosuspension; 10 mg/kg melanin equivalent). Serial retro-orbital blood samples (0.3 mL) were collected pre-dose and at 0.25, 0.5, 1, 2, 4, 8, 12, 24 h post-dose, with plasma replaced by 5% glucose-saline. Plasma, isolated by centrifugation (3000×g, 10 min, 4°C), was stored at -80°C.

Melanin levels were determined post-acetonitrile-TFA (2:1) protein precipitation via UV spectrophotometry (λ_{max} 340 nm) against a validated plasma standard curve (0.1-50 µg/mL; $r^2 > 0.99$). Phoenix WinNonlin® v8.3 enabled non-compartmental analysis for C_{max}, $AUC_{0-\infty}$, $t_{1/2}$, Cl, V_d, MRT. One-way ANOVA with Tukey's post-hoc test assessed differences ($p<0.05$).

Results And Discussion

Central Composite Design and Experimental Responses

The CCD matrix and experimentally observed responses are presented in Table 2. Particle size varied from 80 to 130 nm, whereas zeta potential ranged from 10 to 30 mV across the experimental formulations. The variation in both responses demonstrated the influence of melanin and lecithin concentrations on the physicochemical characteristics of the formulation. Notably, the center-point formulations containing 15 mg melanin and 7.5 mg lecithin produced identical particle size and zeta potential values of 100 nm and 30 mV, respectively, indicating reproducibility at the center of the experimental domain.

Table 2: Central composite design matrix and experimentally observed responses

Run	Melanin (mg)	Lecithin (mg)	Particle size (nm)	Zeta potential (mV)
1	7.92893	7.5	100	30
2	20.000	10.0	98	20
3	15.000	7.5	100	30
4	20.000	5.0	80	30
5	22.0711	7.5	88	30
6	15.000	3.96447	100	24
7	15.000	11.0355	88	10
8	10.000	10.0	98	10
9	15.000	7.5	100	30
10	10.000	5.0	130	30

Statistical Analysis of Particle Size

The quadratic model developed for particle size was statistically significant, with an F-value of 70.57 and p = 0.0005,

demonstrating that the fitted model accounted for a significant proportion of the observed variation. The model exhibited a high R^2 of 0.9888 and an adjusted R^2 of 0.9748, indicating that 98.88% of the experimental variation in particle size was explained by the model. All five model terms, namely melanin (A), lecithin (B), the A×B interaction, A^2, and B^2, were statistically significant ($p < 0.05$). The significant interaction term indicates that the influence of one formulation variable on particle size was dependent on the concentration of the other variable (Table 3).

Table 3: ANOVA of the quadratic model for particle size

Source	Sum of squares	df	Mean square	F-value	p-value
Model	2059.55	5	411.91	70.57	0.0005
A—Melanin	784.63	1	784.63	134.43	0.0003
B—Lecithin	669.74	1	669.74	114.75	0.0004
AB	617.93	1	617.93	105.87	0.0005
A^2	684.21	1	684.21	117.23	0.0004
B^2	989.45	1	989.45	169.52	0.0002
Residual	23.35	4	5.84	—	—
Lack of fit	18.85	1	18.85	12.56	0.0382
Pure error	4.50	3	1.50	—	—
Cor. total	2082.90	9	—	—	—

The quadratic model in coded factors was

$$Y_1 = 96.13 + 15.29A + 14.09B + 8.99AB + 19.77A^2 - 7.85B^2$$

The positive coefficients for A, B, and AB indicate positive contributions of these terms to the modelled particle-size response, whereas the significant quadratic coefficients demonstrate nonlinear behavior within the investigated formulation region. The model standard deviation was 2.42 nm, with a CV of 2.46% and adequate precision of 33.1444, indicating a strong signal relative to experimental noise (Table 4).

Table 4: Fit statistics of the particle-size model

Parameter	Value
Standard deviation	2.42
Mean	98.10
CV (%)	2.46
R^2	0.9888
Adjusted R^2	0.9748
Predicted R^2	−4.7852
Adequate precision	33.1444

Despite the high R^2 and adjusted R^2 values, the particle-size model exhibited a significant lack of fit ($p = 0.0382$). Furthermore, the predicted R^2 was negative (−4.7852), indicating poor predictive performance outside the experimental observations. Therefore, the model should be considered a strong statistical description of the available experimental data rather than a validated predictive model. Independent confirmation experiments are required before the optimized formulation can be considered experimentally validated (Figure 1 and 2).

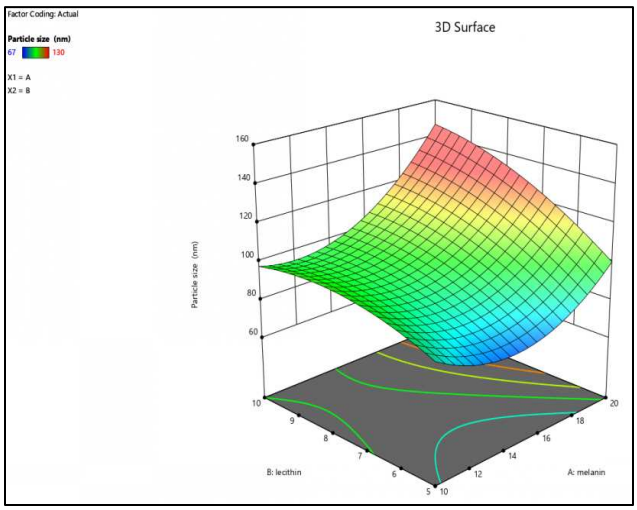


Figure 1: Three-dimensional response-surface plot illustrating the combined effects of melanin and lecithin concentrations on particle size.

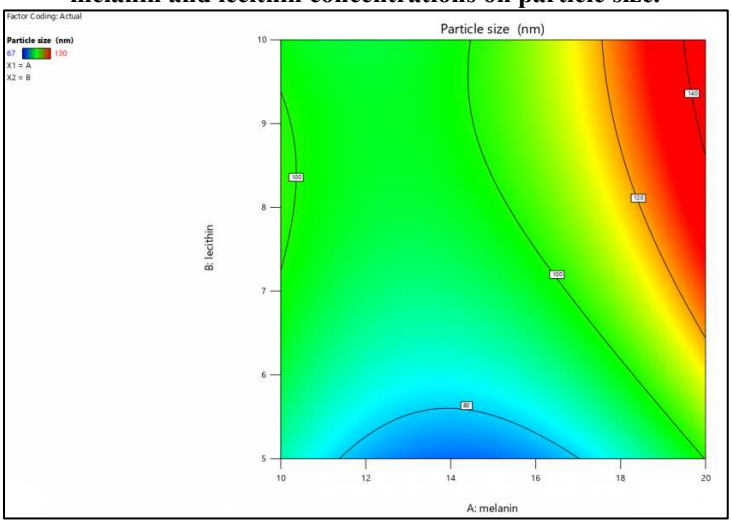


Figure 2: Contour plot illustrating the interactive effects of melanin and lecithin concentrations on particle size.

Statistical Analysis of Zeta Potential

The quadratic model for zeta potential was highly significant, with an F-value of 2508.13 and $p < 0.0001$. The model explained 99.97% of the observed variation, as demonstrated by an R^2 of 0.9997 and adjusted R^2 of 0.9993. All five model terms were statistically significant at $p < 0.0001$. Among the model terms, the A×B interaction exhibited the highest F-value (3868.67), demonstrating the pronounced influence of the combined effects of melanin and lecithin concentrations on zeta potential (Table 5).

Table 5: ANOVA of the quadratic model for zeta potential

Source	Sum of squares	df	Mean square	F-value	p-value
Model	382.28	5	76.46	2508.13	<0.0001
A—Melanin	50.08	1	50.08	1643.01	<0.0001
B—Lecithin	29.13	1	29.13	955.72	<0.0001
AB	117.93	1	117.93	3868.67	<0.0001
A^2	34.42	1	34.42	1129.18	<0.0001
B^2	13.82	1	13.82	453.32	<0.0001
Residual	0.1219	4	0.0305	—	—
Lack of fit	0.1219	1	0.1219	—	—

Pure error	0.0000	3	0.0000	—	—
Cor. total	382.40	9	—	—	—

The quadratic equation in coded factors was:

$$Y_2 = 30.52 - 3.86A - 2.94B - 3.93AB - 4.43A^2 + 0.9282B^2$$

The zeta-potential model exhibited a standard deviation of 0.1746 mV and a CV of 0.6148%, indicating low experimental variability. The adequate precision of 161.8471 demonstrated a strong signal relative to noise. The predicted R^2 was 0.7963, indicating substantially better predictive capability than the particle-size model, although confirmation experiments remain necessary. Because the pure error was zero, Design-Expert® did not provide a conventional F-test and p-value for lack of fit (Table 6 and Figure 3 and 4).

Table 6: Fit statistics of the zeta-potential model

Parameter	Value
Standard deviation	0.1746
Mean	28.40
CV (%)	0.6148
R^2	0.9997
Adjusted R^2	0.9993
Predicted R^2	0.7963
Adequate precision	161.8471

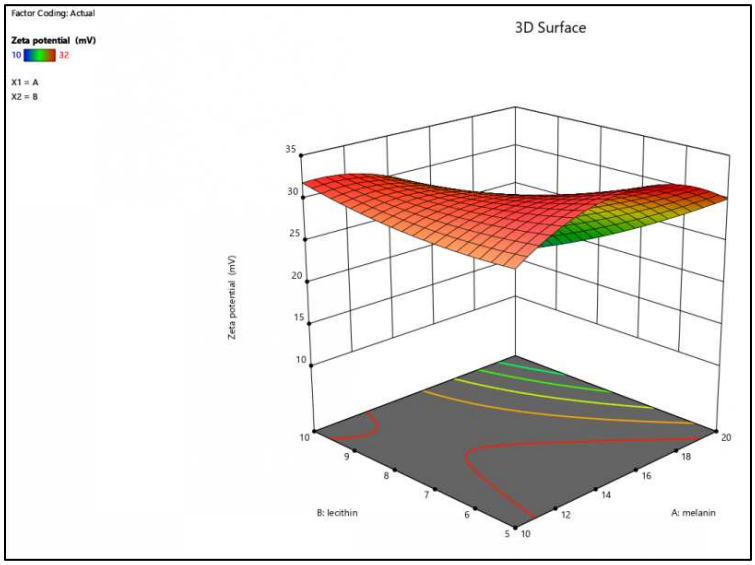


Figure 3: Three-dimensional response-surface plot illustrating the combined effects of melanin and lecithin concentrations on zeta potential.

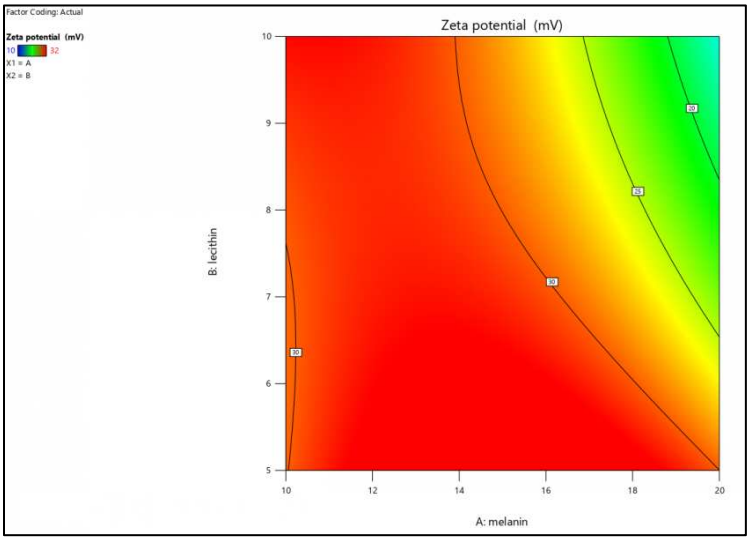


Figure 4: Contour plot illustrating the interactive effects of melanin and lecithin concentrations on zeta potential.

Regression Equations in Terms of Actual Factors

For practical prediction using the original formulation concentrations, the Design-Expert® equations were: **Particle size:** $Y_1 = 196.09190 - 26.05414A + 13.69990B + 0.719206AB + 0.790604A^2 - 1.25673B^2$. **Zeta potential:** $Y_2 = -15.96260 + 6.90366A + 1.30941B - 0.314191AB - 0.177328A^2 + 0.148517B^2$. where A represents melanin concentration and B represents lecithin concentration in their original units.

Numerical Optimization and Selection of the Optimized Formulation

Numerical optimization was performed using the desirability-function approach. Melanin and lecithin were constrained within 10–20 and 5–10 mg, respectively, with both formulation factors assigned minimization goals. Particle size was minimized, whereas zeta potential was maximized. Equal lower and upper weights of 1 and an importance value of 3 were assigned to all criteria (Table 7).

Table 7: Optimization criteria used for numerical optimization

Variable/Response	Goal	Lower	Upper	Importance
Melanin (mg)	Minimize	10	20	3
Lecithin (mg)	Minimize	5	10	3
Particle size (nm)	Minimize	67	130	3
Zeta potential (mV)	Maximize	10	32	3

Six feasible solutions were generated, with overall desirability values ranging from 0.889 to 0.910. The highest desirability of 0.910 was obtained for 11.366 mg melanin and 5.000 mg lecithin, corresponding to predicted particle size and zeta potential values of 80.052 nm and 32.000 mV, respectively. This formulation was therefore selected as the model-predicted optimized formulation (Table 8 and Figure 5 and 6).

Table 8: Numerical optimization solutions generated by Design-Expert®.

Solution	Melanin (mg)	Lecithin (mg)	Predicted particle size (nm)	Predicted zeta potential (mV)	Desirability
1	11.366	5.000	80.052	32.000	0.910
2	11.412	5.000	79.844	32.060	0.909
3	11.209	5.000	80.775	31.791	0.908
4	11.150	5.000	81.054	31.712	0.908

5	10.995	5.000	81.825	31.493	0.906
6	10.199	5.000	86.358	30.241	0.889

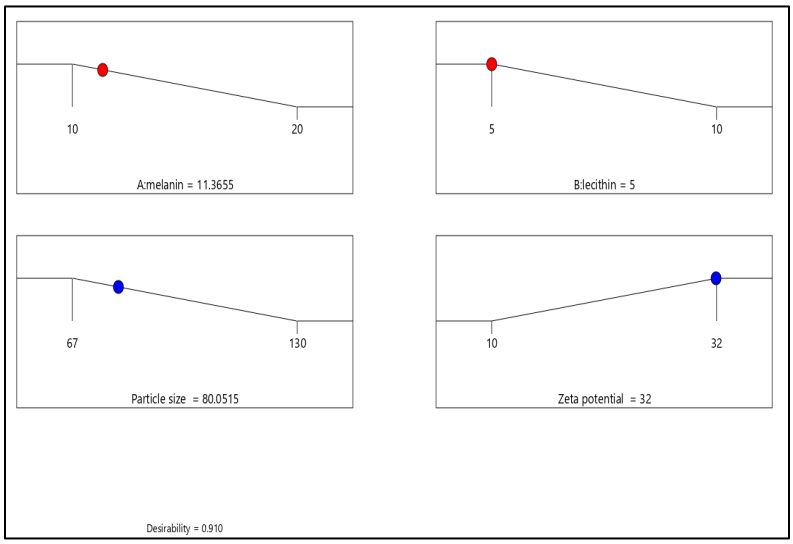


Figure 5: Numerical optimization/desirability ramp generated using Design-Expert® showing the selected formulation composition and predicted responses.

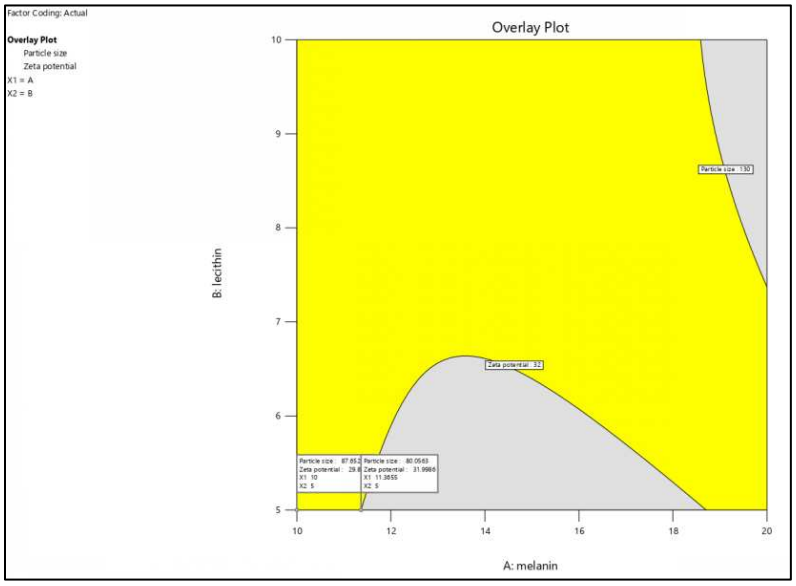


Figure 6. Overlay plot showing the feasible design region for simultaneous optimization of particle size and zeta potential.

Optimized Formulation

The numerical optimization identified 11.366 mg melanin and 5.000 mg lecithin as the optimum formulation composition, with a model-predicted particle size of 80.052 nm, predicted zeta potential of 32.000 mV, and overall desirability of 0.910. For final experimental validation, the optimized formulation should be prepared independently and characterized for particle size and zeta potential. Importantly, the optimized values should presently be reported as model-predicted responses, rather than experimentally validated values. This distinction is particularly important because the particle-size model exhibited significant lack of fit and a negative predicted R^2, while the zeta-potential model, despite its excellent fit, had a predicted R^2 of 0.7963. Experimental confirmation is therefore required to establish agreement between predicted and observed responses and to substantiate the predictive validity of the optimization model.

Synthesis and Characterisation of M-C-L-M-NPs

UV spectroscopy analysis of M-C-L-M-NPs

UV spectroscopy analysis of M-C-L-M-NPs demonstrated strong absorbance in the UV-visible range, particularly between 220 nm and 400 nm. The optical density increased sharply from OD220 (5.831) to OD400 (1.785), indicating high melanin content and successful coating. Absorbance peaks in this region are characteristic of melanin and confirm its presence on the nanoparticles (Figure 7). The gradual decrease in absorbance beyond 400 nm suggests minimal light scattering or absorption by the lipid core and magnetic material. These spectral features confirm both the integrity and uniform coating of melanin on the lipid magnetic nanoparticles, which is essential for their functional application.

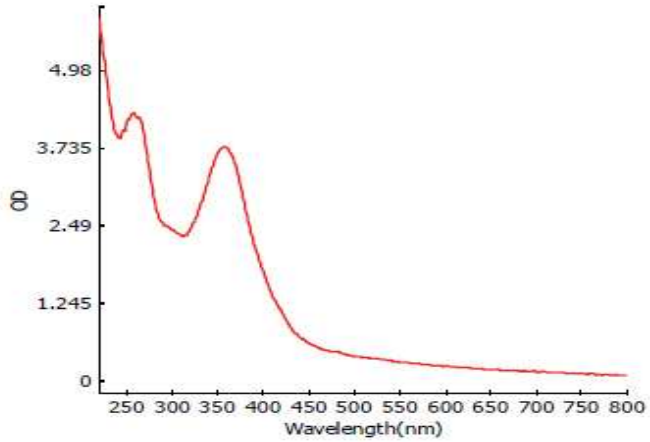


Figure 7: UV spectroscopy analysis of M-C-L-M-NPs.

IR spectroscopy analysis of M-C-L-M-NPs

Infrared (IR) spectroscopy of M-C-L-M-NPs reveals distinct absorption bands indicative of the material's composition and successful coating. Key peaks are observed at 3,365–3,302cm⁻¹ (O–H and N–H stretching), confirming the presence of hydroxyl and amine groups from melanin and possibly lipid components. A prominent band at 2,985cm⁻¹ is associated with C–H stretching, signifying aliphatic chains from the lipid layer. The strong absorption at 1,643cm⁻¹ corresponds to C=O stretching (amide I), reflecting melanin's characteristic indole structure. Peaks between 1,151–1,072cm⁻¹ suggest C–O or P=O stretching, evidencing phospholipid presence (Figure 8). These analyses confirm successful integration of melanin and lipid onto magnetic cores and the structural integrity of M-C-L-M-NPs.

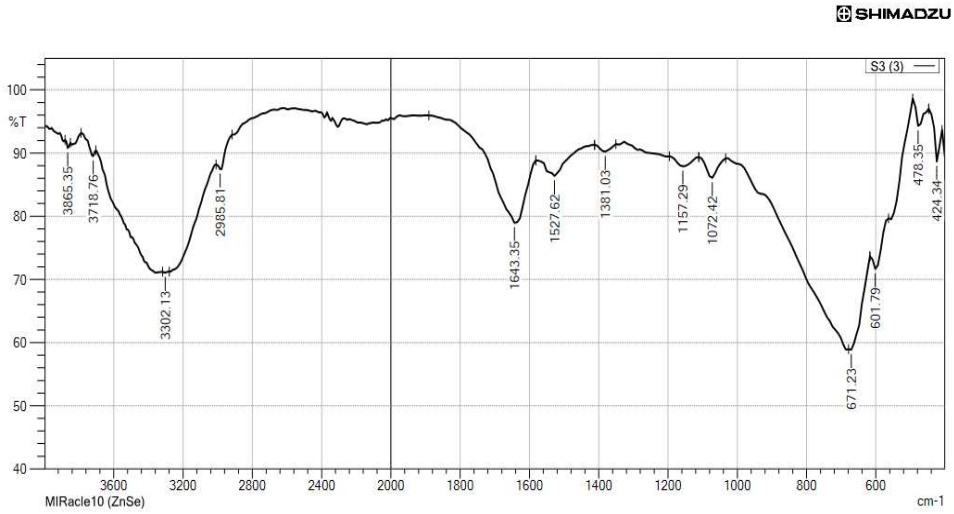


Figure 8: Infrared (IR) spectroscopy of M-C-L-M-NPs.

FE-SEM and HR-TEM of M-C-L-M-NPs

FE-SEM and HR-TEM analyses confirmed the morphology and size distribution of M-C-L-M-NPs. FE-SEM images revealed that the nanoparticles exhibit a rough surface and nearly spherical morphology, with primary particle clusters displaying consistent texture at the nanometric scale. HR-TEM provided detailed insights, confirming that the nanoparticles are composed of discrete, well-dispersed entities with a core-shell architecture (Figure 9). The measured diameters from HR-TEM ranged approximately from 24nm to 63nm, consistent with the size ranges observed in FE-SEM. These findings confirm the successful formation of M-C-L-M-NPs with a uniform, nanoscale structure suitable for biomedical applications.

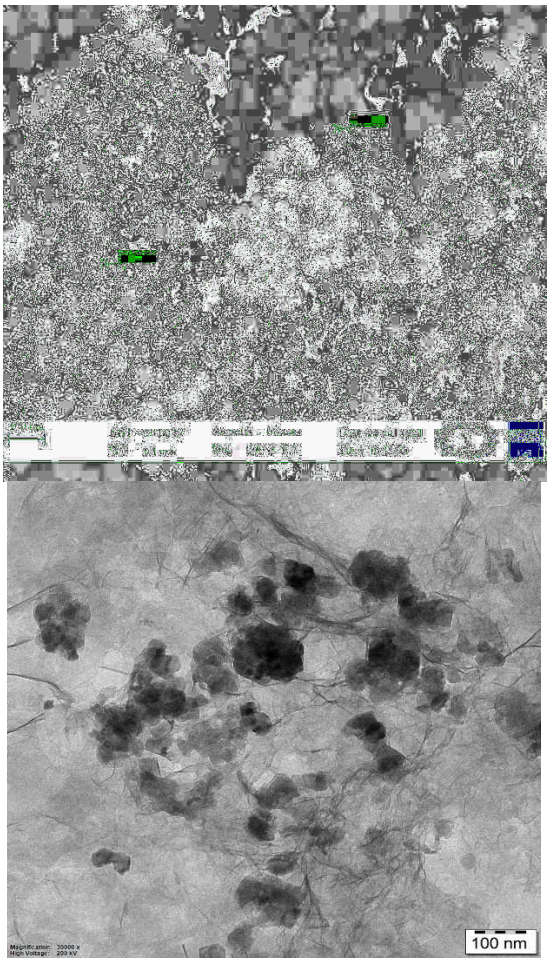


Figure 9: FE-SEM and HR-TEM analyses of M-C-L-M-NPs.

Zeta potential and Zeta Size analysis of the M-C-L-M-NPs

M-C-L-M-NPs exhibited a hydrodynamic diameter with a Z-average value of 89.2nm, as measured by dynamic light scattering, and displayed a moderate polydispersity index (PdI) of 0.31, confirming a relatively uniform particle size distribution (Figure 10A). The intensity-based analysis revealed three primary peaks, with the most significant proportion of particles centred around 91.5nm, and minor populations at smaller (35.9nm) sizes. Zeta potential measurements showed a mean value of -30.2mV, indicating good colloidal stability and sufficient surface charge to prevent aggregation (Figure 10B). The nanoscale size and stable zeta potential combination suggests these nanoparticles are well-suited for biomedical applications, benefiting from stability and dispersibility in aqueous environments.

		Size (d.nm):	% Intensity:	St Dev (d.n...
Z-Average (d.nm): 89.2	Peak 1:	98.5	91.5	12.1
PdI: 0.31	Peak 2:	35.88	5.3	6.118
Intercept: 0.91	Peak 3:	517	3.5	488.9
Result quality : Good				

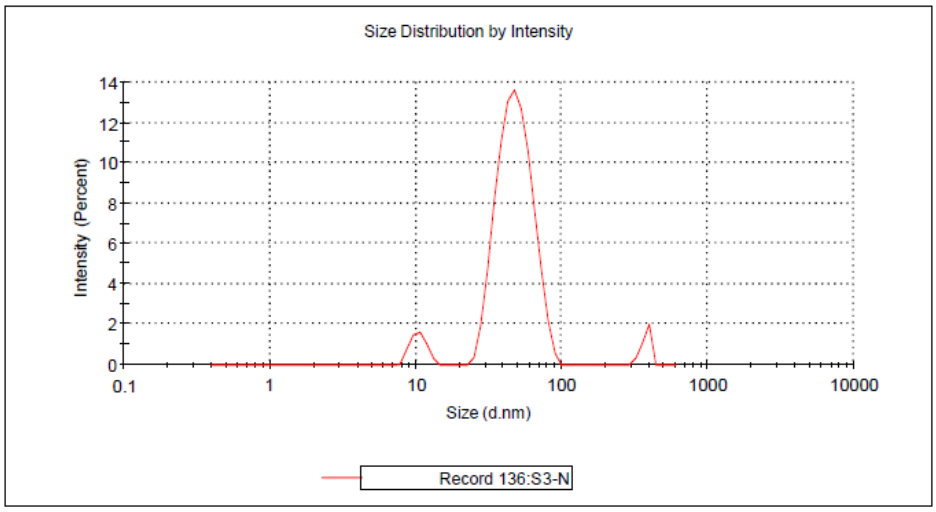


Figure 10A: Zeta size analysis of the M-C-L-M-NPs

		Mean (mV)	Area (%)	St Dev (mV)
Zeta Potential (mV): -30.2	Peak 1:	-30.2	100.0	6.12
Zeta Deviation (mV): 7.12	Peak 2:	0.00	0.0	0.00
Conductivity (mS/cm): 1.16	Peak 3:	0.00	0.0	0.00
Result quality : Good				

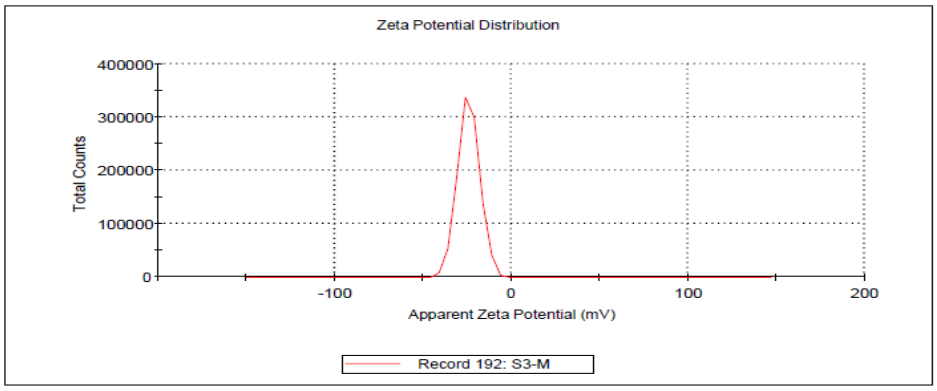


Figure 10B: Zeta potential analysis of the M-C-L-M-NPs.

BET Surface Area and Pore Structure Analysis of M-C-L-M-NPs.

BET surface area analysis of melanin-coated lipid magnetic nanoparticles revealed a specific surface area of approximately 96.9 m^2/g, indicating high porosity and substantial external surface for interaction. Nitrogen adsorption-desorption isotherms displayed a typical Type IV curve, characteristic of mesoporous materials, supporting efficient gas uptake and release (Figure 11). The t-plot and BJH analyses showed the presence of both micropores and mesopores, with a significant pore volume and a range of pore diameters, optimizing the material for biomedical and drug delivery applications. The measured surface characteristics confirm that the synthesis method effectively produces nanoparticles with extensive accessible surface and tailored porosity.

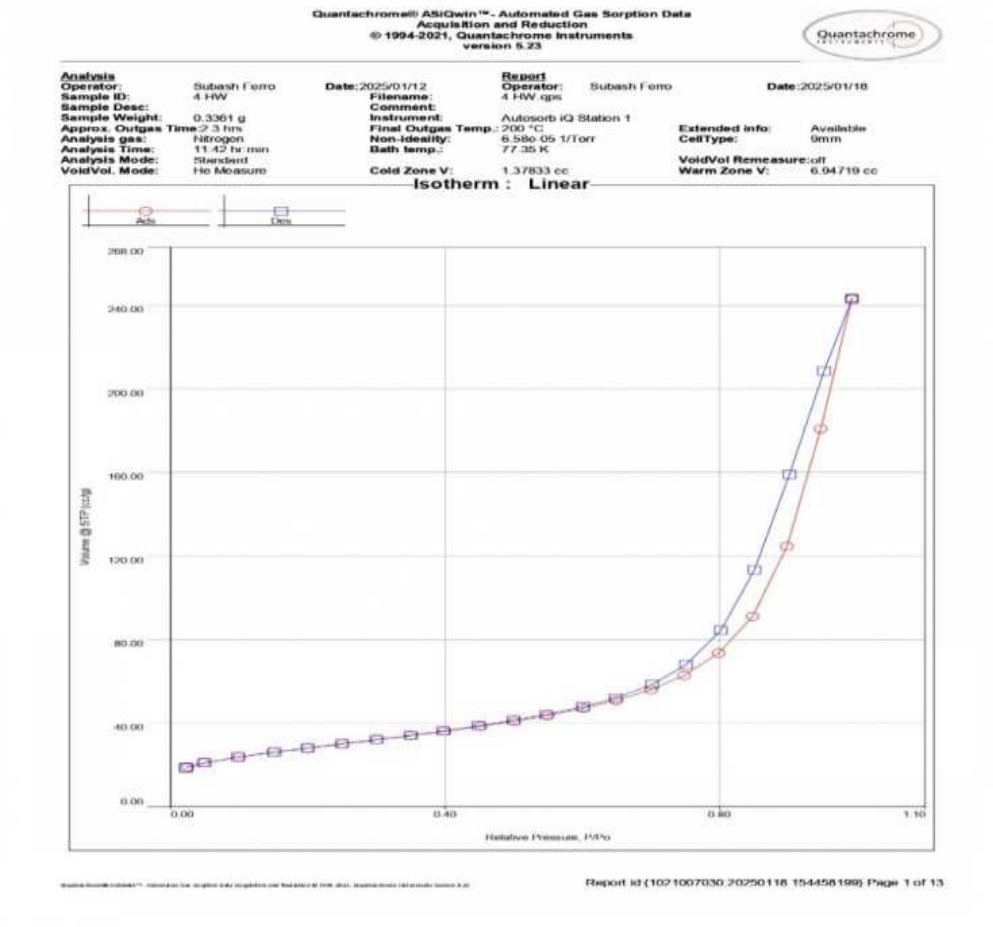


Figure 11: BET surface area and pore structure analysis of M-C-L-M-NPs.

ICP OES Calibration and Iron Quantification of M-C-L-M-NPs

ICP OES analysis of melanin-coated lipid magnetic nanoparticles quantified iron content using the Fe 259.940 nm line intensity. The sample measurements produced a mean intensity of 84.0 with an RSD of 5.1% and SD of 4.2. Iron standard intensities ranged from 1,958 (RSD 0.1%) to 25,462 (RSD 0.6%), demonstrating instrument reliability and calibration accuracy. Blank and wash solutions provided mean intensities of 86.0 and 85.7, respectively, confirming low background interference. These values confirm reliable detection and significant iron incorporation within the nanoparticles, validating the synthesis protocol and ensuring the magnetic core's presence for intended biomedical applications.

***In Vitro* Anticancer Activity of M-C-L-M-NPs Against SK-MEL-3 Cells**

Dose-dependent inhibition of SK-MEL-3 cell viability by M-C-L-M-NPs

The in vitro evaluation of M-C-L-M-NPs against SK-MEL-3 human melanoma cells demonstrates substantial anticancer efficacy. Morphological analysis shows that, compared to untreated controls, treated SK-MEL-3 cells exhibit significant reductions in cell density and alterations in cell morphology at increasing nanoparticle concentrations, indicating dose-dependent cytotoxicity (Figure 12A and 12B). Quantitative analysis further validates these effects; inhibition assays reveal an apparent concentration-dependent inhibition of cell viability, with the inhibition percentage rising steadily with higher nanoparticle doses. The calculated IC_{50} value of approximately 19.1±1.5 µg/ml supports the nanoparticles' potency against melanoma cells. These results suggest that M-C-L-M-NPs effectively induce cytotoxicity, likely through enhanced cellular uptake and induction of apoptotic pathways, as described in studies on melanin-based and lipid nanoparticle systems. The apoptotic AO/EB staining confirmed that SK-MEL-

3 cells were dead. Treatment with increasing concentrations of M-C-L-M-NPs exhibited a strong, dose-dependent cytotoxic effect. Control cells appeared healthy and densely populated (green). Cells treated with 10 µg showed reduced density, and at 20 µg, most cells stained yellow, indicating significant apoptosis and cell death (Figure 12C). Such targeted nanocarrier systems offer potent anticancer activity and may minimize toxicity to healthy cells, supporting further investigation for melanoma therapy.

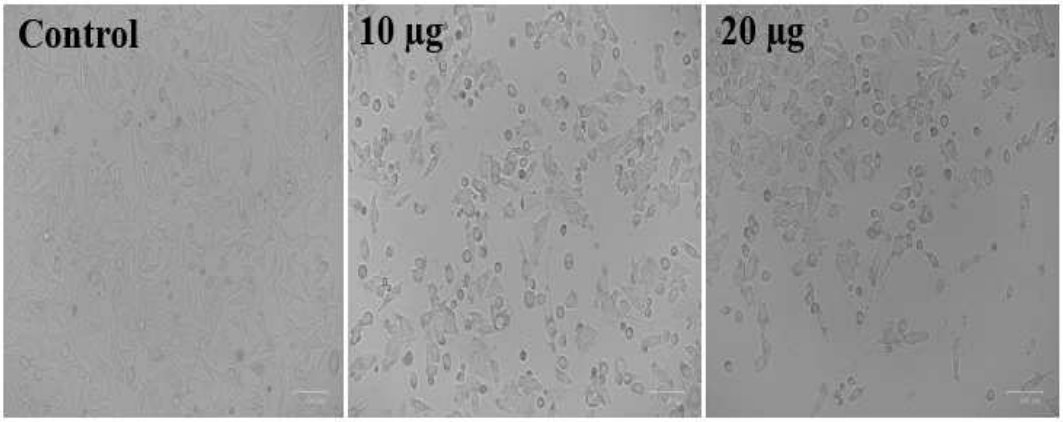


Figure 12A: Morphological changes in SK-MEL-3 cells after treatment with M-C-L-M-NPs at 10 µg and 20 µg compared to untreated control.

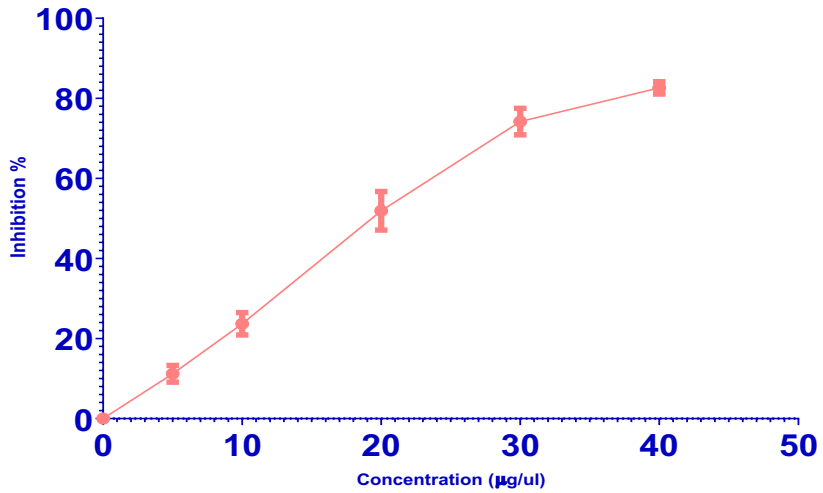


Figure 12B: Dose-dependent inhibition of SK-MEL-3 cell viability by M-C-L-M-NPs, shown as inhibition percentage versus nanoparticle concentration.

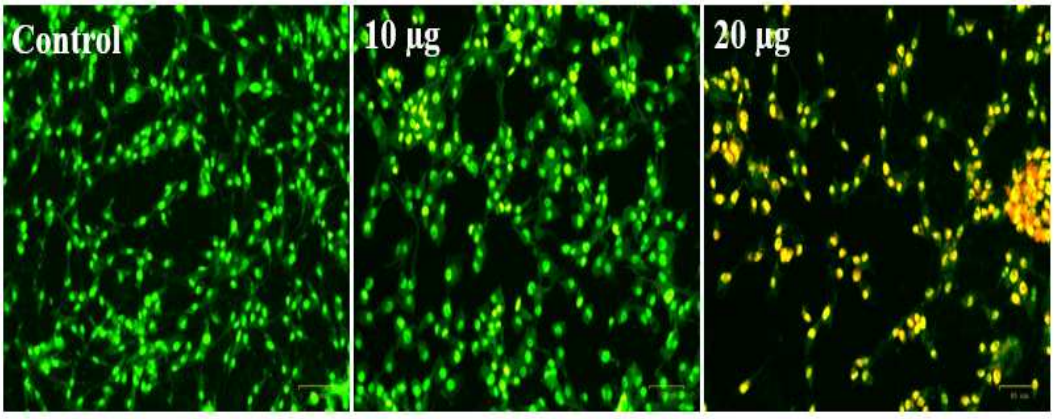
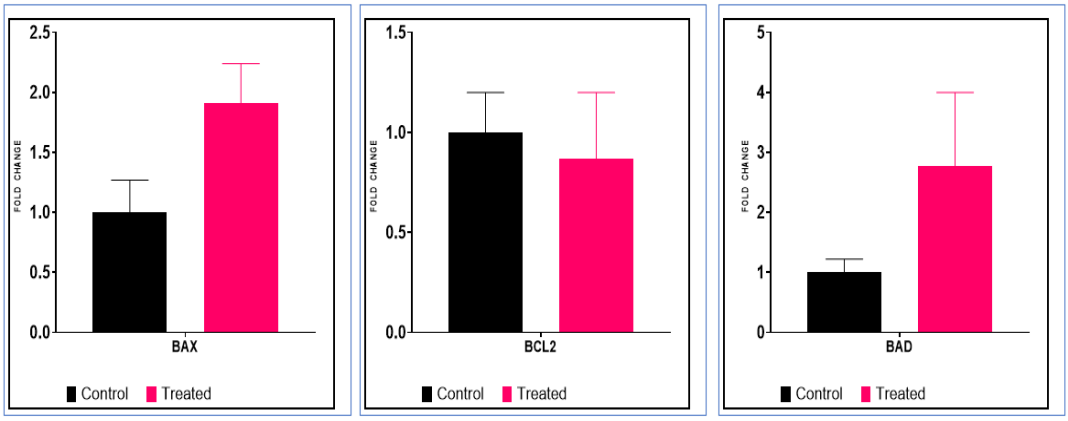


Figure 12C: Fluorescent staining illustrating apoptotic changes in SK-MEL-3 cells following treatment with M-C-L-M-NPs (Control, 10 µg, and 20 µg).

Quantitative Real-time PCR (Gene expression)

Gene expression analysis of SK-MEL-3 cells treated with M-C-L-M-NPs, as depicted in the graphs, shows a pronounced activation of apoptotic pathways. There is a significant upregulation of pro-apoptotic genes BAX (1.91-fold) and BAD (2.77-fold) in treated cells compared to controls, while the anti-apoptotic gene BCL2 is slightly downregulated (relative concentration 0.87). The increased BAX/BCL2 and BAD/BCL2 ratios strongly indicate a shift toward apoptosis, supporting the cytotoxic effects observed in earlier assays (Figure 13). These molecular changes confirm that M-C-L-M-NP treatment effectively induces apoptosis in SK-MEL-3 melanoma cells, validating the nanoparticles' mechanism of anticancer action via pro-apoptotic gene modulation.



Replicate Name	GOI CT	Norm. CT	Relative Conc.	SD
C	13.44	13.49	1	0.27
T	12.94	13.92	1.91	0.33

Replicate Name	GOI CT	Norm. CT	Relative Conc.	SD
C	9.91	13.49	1	0.2
T	10.54	13.92	0.87	0.33

Replicate Name	GOI CT	Norm. CT	Relative Conc.	SD
C	10.86	13.49	1	0.22
T	9.82	13.92	2.77	1.23

Figure 13: Fold change in pro-apoptotic BAX, BCL2 and BAD gene expression in SK-MEL-3 cells after M-C-L-M-NP treatment compared to control.

Gene Expression Changes in SK-MEL-3 Cells Treated with M-C-L-M-NPs

The gene expression profile depicted in the graph shows that treatment with M-C-L-M-NPs significantly alters apoptotic and survival pathways in SK-MEL-3 cells. There is a pronounced upregulation of the pro-apoptotic gene BAD (nearly threefold increase) and a marked downregulation of the survival gene AKT in treated cells relative to controls. BCL2, an anti-apoptotic gene, also shows a slight decrease after treatment. Increased BAD expression and reduced AKT and BCL2 levels suggest a shift toward apoptosis and decreased cell survival mechanisms (Figure 14). These molecular changes further corroborate the observed cytotoxicity and apoptosis in nanoparticle-treated melanoma cells, supporting the therapeutic potential of M-C-L-M-NPs.

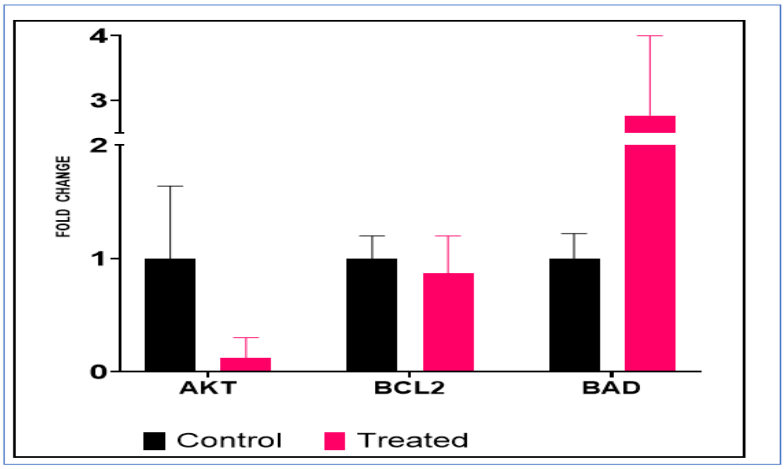


Figure 14: Relative Fold Change in AKT, BCL2, and BAD Gene Expression in SK-MEL-3 Cells After Treatment with M-C-L-M-NPs.

Melanin-Conjugated Magnetic nanosuspension

***In-Vitro* drug release study of M-C-L-M-NPs-Suspension**

The *in-vitro* release profile of melanin from the M-C-L-M-NPs suspension demonstrated a gradual increase in cumulative melanin release over the 24-h study period (Table 9). An initial release of 6.27 ± 0.21% was observed at 0.5 h, increasing to 9.97 ± 0.21% at 1 h. The cumulative release subsequently increased progressively to 15.83 ± 0.25% at 2 h, 25.70 ± 0.30% at 4 h, 35.17 ± 0.31% at 6 h, and 44.60 ± 0.40% at 8 h. At 12 h, the cumulative melanin release reached 58.97 ± 0.40%, followed by a further increase to 75.20 ± 0.40% at 24 h. The relatively low standard deviations observed among the triplicate measurements indicate good reproducibility of the release measurements. The progressive release pattern indicates gradual liberation of melanin from the M-C-L-M-NPs suspension over the investigated period. (Figure 15).

Table 9: *In-vitro* drug release profile of M-C-L-M-NPs-Suspension.

Time (h)	Trial	Trial 2	Trial 3	Mean ± SD (%)
0.5	6.2	6.5	6.1	6.27 ± 0.21
1	9.8	10.2	9.9	9.97 ± 0.21
2	15.6	16.1	15.8	15.83 ± 0.25
4	25.4	26.0	25.7	25.70 ± 0.30
6	34.9	35.5	35.1	35.17 ± 0.31
8	44.2	45.0	44.6	44.60 ± 0.40
12	58.6	59.4	58.9	58.97 ± 0.40
24	74.8	75.6	75.2	75.20 ± 0.40

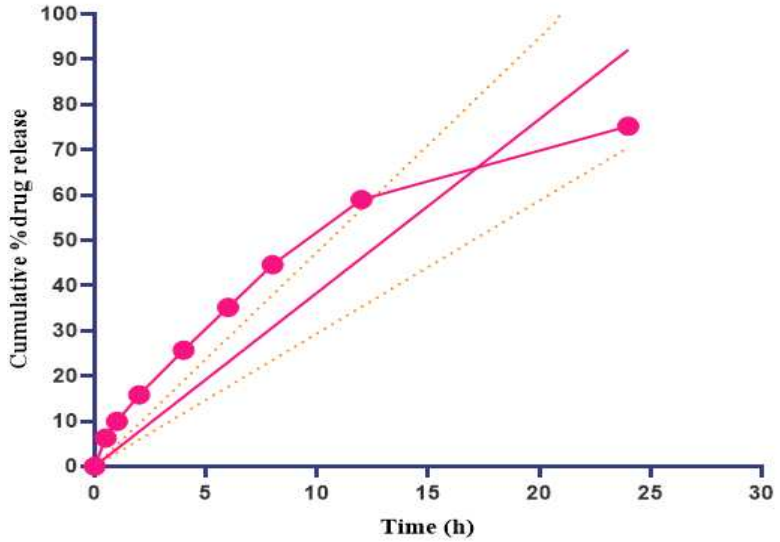


Figure 15: *In-vitro* drug release profile of M-C-L-M-NPs-Suspension in phosphate buffer (pH 7.4) over 24 h.

***In-vitro* Drug release kinetics**

The *in-vitro* melanin release data from the M-C-L-M-NPs suspension were fitted to zero-order, first-order, Higuchi, and Korsmeyer–Peppas kinetic models (Figure 16). The zero-order model showed a moderate correlation with the experimental release data (R^2 =0.909), indicating that the release profile was not adequately described by a constant-rate release model. The first-order model exhibited a comparatively lower correlation(R^2=0.694), suggesting a poorer fit to the observed release profile. The Higuchi model showed a strong correlation (R^2=0.987), indicating that diffusion contributed substantially to the observed melanin release. Among the evaluated models, the Korsmeyer–Peppas model exhibited the highest correlation (R^2 =0.993), with a release exponent (n) of 0.673. Under the applicable assumptions of the Korsmeyer–Peppas model, the (n) value suggests anomalous/non-Fickian release behaviour, indicating that the release may involve a combination of diffusion and other formulation-dependent processes. The kinetic analysis indicates that the Korsmeyer–Peppas model provided the best empirical fit to the experimental release data, while the Higuchi model also demonstrated a strong association with the observed release profile

.

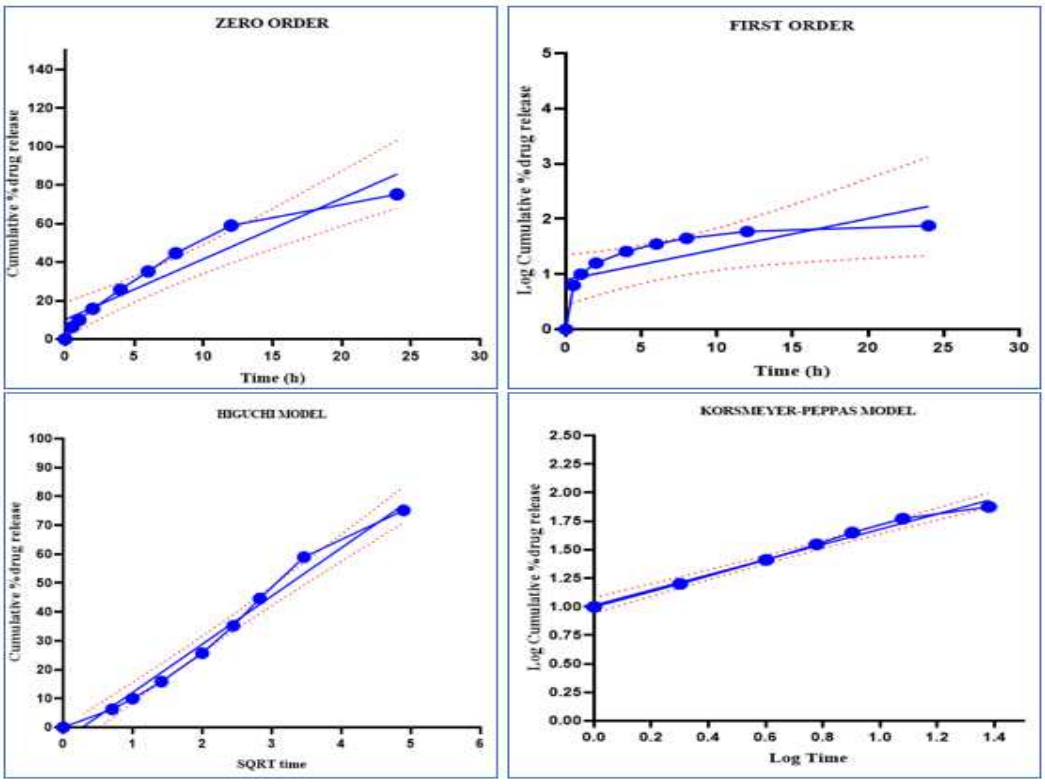


Figure 16: Drug release kinetic model fitting plots (zero-order, first-order, Higuchi, and Korsmeyer–Peppas models) for M-C-L-M-NPs-Suspension.

Sterility Testing Melanin-Conjugated Magnetic Nanosuspension

Sterility evaluation results for the melanin-conjugated magnetic nanoparticle suspension, conducted per Indian Pharmacopoeia (IP) and United States Pharmacopoeia (USP) standards. In Fluid Thioglycolate Medium incubated at 30–35°C, no turbidity developed over 14 days. Soybean Casein Digest Medium maintained at 20–25°C showed complete absence of microbial growth throughout the 14-day observation period. These findings confirm no viable bacterial or fungal contamination, verifying the formulation's sterility and suitability for safe intravenous administration in pharmacokinetic studies.

Aute toxicity study of M-C-L-M-NPs-Suspension

Acute toxicity monitoring of the M-C-L-M-NPs suspension revealed no treatment-related adverse effects. Animals exhibited normal behavior and physiological functions throughout the observation period, with no tremors or convulsions (Table 10). Parameters including salivation, sleep, gastrointestinal status, skin, eyes, respiration, circulation, autonomic responses, and motor activity remained within normal limits.

Table 10: Observation parameters in acute toxicity of M-C-L-M-NPs-Suspension.

Parameters	M-C-L-M-NPs-Suspension
Tremors	Not observed
Convulsions	Not observed
Salivation	Normal
Sleep	Normal
Diarrhoea	Normal
Lethargy	Normal

Skin and Fur	Normal
Eyes	Normal
Respiratory	Normal
Circulatory	Normal
Autonomic and CNS	Normal
Motor activity	Normal

Histopathology observation of metabolic organs liver and Kidney

Histopathological analysis of liver treated animals with M-C-L-M-NPs-Suspension demonstrated normal hepatic tissue organization. The hepatocytes appeared healthy with clear cytoplasm and centrally located nuclei, and the hepatic sinusoids were well maintained. No signs of cellular degeneration, necrosis, or inflammatory infiltration were observed. The normal appearance of the central vein and portal areas further confirms the absence of hepatocellular injury caused by the extract. Kidney tissues of M-C-L-M-NPs-Suspension treated animals showed normal histological architecture (Figure 17). The glomeruli and renal tubules were structurally intact, and there was no indication of edema. The interstitial spaces appeared normal, confirming that the extract did not impair renal function or structure during acute exposure.

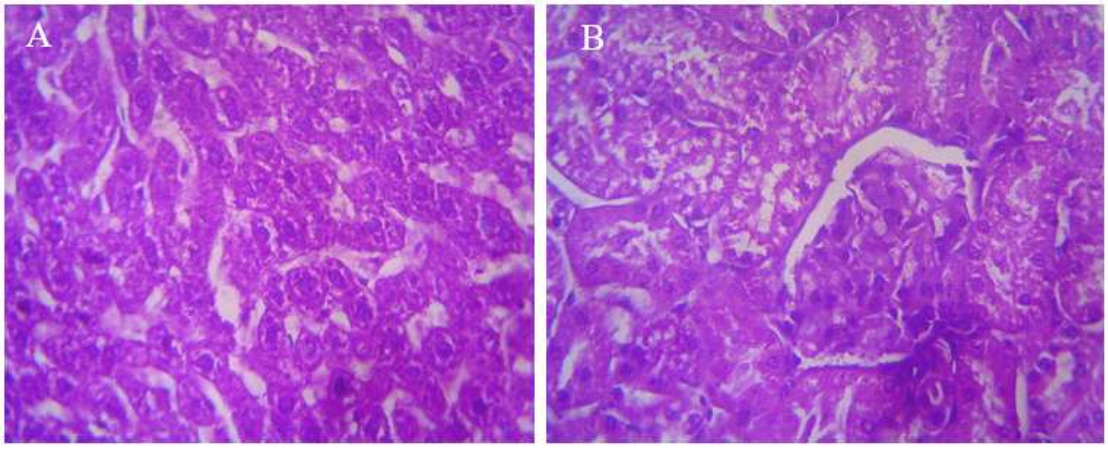


Figure 17: A: Histopathological observation of liver treated animals with M-C-L-M-NPs-Suspension. B: Histopathological observation of kidney treated animals with M-C-L-M-NPs-Suspension.

***In-vivo* Pharmacokinetic Studies of M-C-L-M-NPs-Suspension**

Plasma concentration-time profiles revealed dramatic pharmacokinetic enhancement by MC-MNPs nanosuspension (Group III) versus free melanin (Group II). While pure melanin showed rapid distribution (Cmax 22.6 µg/mL at 1 h) and elimination (undetectable by 24 h), the nanosuspension maintained elevated levels throughout: sustained Cmax (29.6 µg/mL at 4 h), and 10.4 µg/mL detectable at 24 h versus 2.1 µg/mL for free drug. This ~5-fold prolonged exposure reflects magnetic nanoparticle protection against RES clearance, reduced plasma clearance, and expanded volume of distribution (Table 11 and Figure 18). Such superior AUC, extended t½, and biphasic decline validate nanosuspension design for sustained melanin delivery, minimizing dosing frequency for clinical iron chelation applications.

Table 11: Plasma Melanin Concentration-Time Profiles Across Animal Treatment Groups.

Time (h)	Control (Group I)	Melanin (µg/mL) Group II	M-C-L-M-NPs Suspension (µg/mL) (Group III)
0	0	0.0	0.0
0.25	0	12.5	9.8
0.5	0	18.4	15.6
1	0	22.6	21.9
2	0	20.1	27.8
4	0	15.2	29.6
8	0	9.4	24.2
12	0	5.6	18.7
24	0	2.1	10.4

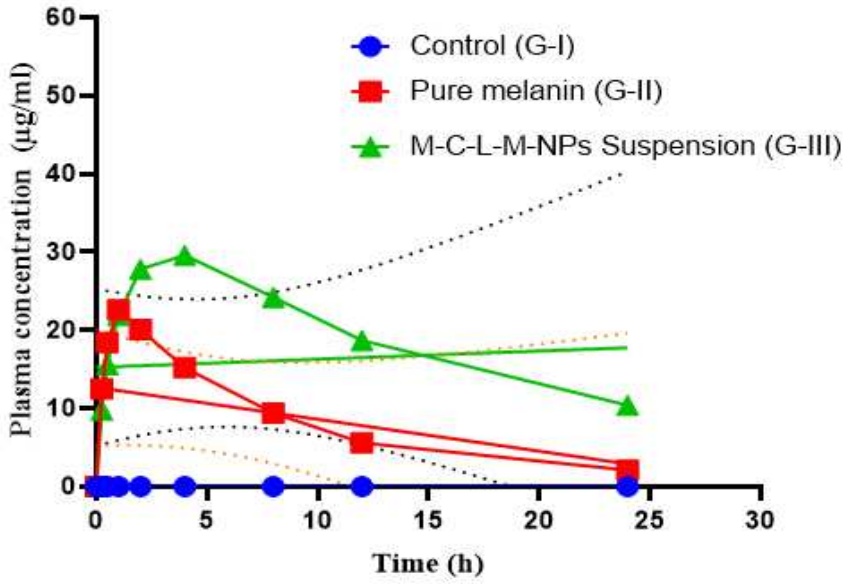


Figure 18: Plasma melanin concentration-time curves after IV administration across experimental groups (Group I: saline control, Group II: free melanin, Group III: MC-MNPs nanosuspension).

Conclusion

The optimized synthesis and detailed characterization of marine bacterial melanin-conjugated magnetic lipid nanoparticles (M-C-L-M-NPs) demonstrate that melanin and phosphatidylcholine concentrations are crucial in determining nanoparticle size and stability. Statistical analysis confirms that higher melanin concentrations enhance colloidal stability by improving zeta potential, while lower phosphatidylcholine levels result in smaller, more uniform nanoparticle attributes vital for biomedical use. Spectroscopic evaluations (UV-Vis and FTIR) confirm successful functionalization and a uniform melanin coating, which is essential for biocompatibility and targeted therapeutic effects. The narrow confidence intervals for particle size and zeta potential reflect process reliability, while broader tolerance intervals indicate robustness for scalability in varied applications. Importantly, in vitro studies against SK-MEL-3 human melanoma cells reveal that M-C-L-M-NPs induce significant, dose-dependent cytotoxicity, confirmed by decreases in cell viability, increased apoptotic morphology, and an IC_{50} value of about 19.1 µg/ml. Gene expression analysis further evidences the induction of apoptosis via upregulation of BAX and BAD and downregulation of BCL2 and AKT. M-C-L-M-NPs-Suspension provided reproducible diffusion-controlled release with minimal burst and 75% liberation at 24 h. Safety was verified by sterility, absence of acute toxicity, and

normal histology. Enhanced exposure, delayed elimination. These findings underscore the anticancer promise of M-C-L-M-NPs as targeted nanocarriers for melanoma treatment and provide a strong, innovative basis for their future development in cancer nanomedicine.

Conflict Of Interest: Nil

Acknowledgement: The authors thank Department of Pharmacy, Annamalai University, Annamalai Nagar, Chidambaram-608002, Tamil Nadu, India.

Data availability: The data produced during this study are available from the corresponding author upon reasonable request

Abbreviations

M-C-L-M-NPs: Melanin-Coated Lipid Magnetic Nanoparticles
NPs: Nanoparticles
SK-MEL-3: A human melanoma cancer cell line
Zeta potential: The electric potential at the slipping plane of a particle in suspension, often used as a measure of colloidal stability
ANOVA: Analysis of Variance
IR spectroscopy: Infrared Spectroscopy
BET: Brunauer–Emmett–Teller
BJH: Barrett–Joyner–Halenda
ICP OES: Inductively Coupled Plasma Optical Emission Spectrometry
OD: Optical Density
SD: Standard Deviation
RSD: Relative Standard Deviation
CI: Confidence Interval
TI: Tolerance Interval

Reference

1. Wang R, Chen Y, Shao X, et al. Burden of Skin Cancer in Older Adults From 1990 to 2021 and Modelled Projection to 2050. *JAMA Dermatol*. 2025;161(7):715-722. doi:10.1001/jamadermatol.2025.1276.
2. Villani A, Potestio L, Fabbrocini G, Scalvenzi M. New Emerging Treatment Options for Advanced Basal Cell Carcinoma and Squamous Cell Carcinoma. *Adv Ther*. 2022;39(3):1164-1178. doi:10.1007/s12325-022-02044-1.
3. Linares MA, Zakaria A, Nizran P. Skin Cancer. *Prim Care*. 2015;42(4):645-659. doi: 10.1016/j.pop.2015.07.006.
4. Wainberg ZA, Weekes CD, Furqan M, et al. Lymph node-targeted, mKRAS-specific amphiphile vaccine in pancreatic and colorectal cancer: phase 1 AMPLIFY-201 trial final results. *Nat Med*. 2025;31(11):3648-3653. doi:10.1038/s41591-025-03876-4.
5. Jensen SE, Pereira DB, Whitehead N, et al. Cognitive-behavioral stress management and psychological well-being in HIV+ racial/ethnic minority women with human papillomavirus. *Health Psychol*. 2013;32(2):227-230. doi:10.1037/a0028160.
6. El-Naggar NE, El-Ewasy SM. Bioproduction, characterization, anticancer and antioxidant activities of extracellular melanin pigment produced by newly isolated microbial cell factories Streptomyces glaucescens NEAE-H. *Sci Rep*. 2017;7:42129. doi:10.1038/srep42129.
7. Ramesh C, Tulasi BR, Raju M, Thakur N, Dufossé L. Marine Natural Products from Tunicates and Their Associated Microbes. *Mar Drugs*. 2021;19(6):308. doi:10.3390/md19060308.
8. Chen T, Yan Y, Zhou X, et al. An antioxidant hydrogel dressing with wound pH indication function prepared based on silanized bacterial nanocellulose crosslinked with beet red pigment extract. *Int J Biol Macromol*. 2024;269(Pt 1):131824. doi: 10.1016/j.ijbiomac.2024.131824.
9. Boudrahem D, Messaoudi O, Balit S, Kecha M, Wink J, Patel CN. Exploring marine-derived bacterial compounds targeting the μ-opioid receptor agonists through metabolic profiling to molecular modeling. *Sci Rep*. 2025;15(1):17196. doi:10.1038/s41598-025-96411-x.
10. Kamran M, Ahad A, Aqil M, Imam SS, Sultana Y, Ali A. Design, formulation and optimization of novel soft nano-carriers for transdermal olmesartan medoxomil delivery: In vitro characterization and in vivo pharmacokinetic assessment. *Int J Pharm*. 2016;505(1-2):147-158. doi:10.1016/j.ijpharm.2016.03.030.
11. Girardet T, Cherraj A, Venturini P, et al. Elaboration of Functionalized Iron Oxide Nanoparticles by Microwave-Assisted Co-Precipitation: A New One-Step Method in Water. *Molecules*. 2024;29(18):4484. doi:10.3390/molecules29184484.
12. Melchior S, Codrich M, Gorassini A, et al. Design and advanced characterization of quercetin-loaded nano-liposomes prepared by high-pressure homogenization. *Food Chem*. 2023;428:136680. doi:10.1016/j.foodchem.2023.136680.

13. Tuzimski T, Petruczynik A, Plech T, et al. Determination of Selected Isoquinoline Alkaloids from *Chelidonium majus*, *Mahonia aquifolium* and *Sanguinaria canadensis* Extracts by Liquid Chromatography and Their In Vitro and In Vivo Cytotoxic Activity against Human Cancer Cells. *Int J Mol Sci*. 2023;24(7):6360. doi:10.3390/ijms24076360.
14. Santos-Rasera JR, Monteiro RTR, de Carvalho HWP. Investigation of acute toxicity, accumulation, and depuration of ZnO nanoparticles in Daphnia magna. *Sci Total Environ*. 2022; 821:153307. doi: 10.1016/j.scitotenv.2022.153307.
15. Li B, Chen X, Qiu W, et al. Synchronous Disintegration of Ferroptosis Defense Axis via Engineered Exosome-Conjugated Magnetic Nanoparticles for Glioblastoma Therapy. *Adv Sci (Weinh)*. 2022;9(17):e2105451. doi:10.1002/advs.202105451.
16. Lee SJ, Kim JJ, Kang KY, Paik MJ, Lee G, Yee ST. Enhanced anti-tumor immunotherapy by silica-coated magnetic nanoparticles conjugated with ovalbumin. *Int J Nanomedicine*. 2019;14:8235-8249. doi:10.2147/IJN.S194352.
17. Graham W, Torbett-Dougherty M, Islam A, Soleimani S, Bruce-Tagoe TA, Johnson JA. Magnetic Nanoparticles and Drug Delivery Systems for Anti-Cancer Applications: A Review. *Nanomaterials (Basel)*. 2025;15(4):285. doi:10.3390/nano15040285.
18. Ebrahim Damavandi S, Banihashemi Jozdani SM, Elyasigorji Z, Vosough M. Bridging cancer therapies: the role of magnetic nanoparticles in combination cancer therapy. *Discov Nano*. 2026;21(1):49. doi:10.1186/s11671-026-04439-3.